ChemComm

COMMUNICATION

View Article Online
View Journal | View Issue

Cite this: *Chem. Commun.*, 2024, **60**, 4946

Received 29th February 2024,
Accepted 9th April 2024

DOI: 10.1039/d4cc00977k

rsc.li/chemcomm

Solvent-free synthesis and chiroptical properties of a C–N axially chiral cruciform dimer of benzo[*b*]phenoxazine†

Shuhei Ishikawa,[a] Daisuke Sakamaki, *[a] Masayuki Gon,[b] Kazuo Tanaka[b] and Hideki Fujiwara *[a]

A novel C–N axially chiral molecule composed of two *tert*-butyl-substituted benzo[*b*]phenoxazine (BPO) was synthesized *via* solvent-free reactions. The absolute configurations of the enantiomers were determined by X-ray single-crystal analysis. The enantiomers had a sufficiently high racemization barrier to ignore racemization at room temperature (149 ± 20 kJ mol^{-1}), and the solutions exhibited dual circularly polarized emissions stemming from fluorescence and phosphorescence of $|g_{CPL}|$ = *ca.* 1 × 10^{-3}.

In recent years, heteroatom-embedded polyaromatic hydrocarbons (PAHs) have attracted increasing interest for use in functional organic materials, such as luminescent materials for organic light-emitting diodes (OLEDs).[1,2] Heteroacenes with amino nitrogen atoms, such as benzo[*b*]phenoxazine (**BPO**) and benzo[*b*]phenothiazine (**BPT**), are not only utilized in dye-sensitized solar cells[3,4] owing to their good electron-donating and photophysical properties but are also gaining renewed interest as organic photoredox catalysts.[5–8] In 2015, we developed a straightforward method for the synthesis of double heterohelicenes, which comprised two heteroacenes with an NH group, such as 6,13-dihydro-6,13-diazapentacene (**DHDAP**),[9] **BPO**,[10] dibenzo[*b*,*i*]phenoxazine (**DBPO**),[9,10] phenothiazine,[11] **BPT**,[12] and phenoselenazine.[13] The key intermediate compounds in this process are the cruciform dimers formed *via* oxidative C–N coupling between the two azaacenes (Fig. 1). Oxidative C–N coupling between symmetric azaacenes, such as **DBPO** and **DHDAP**, gives achiral cruciform dimers with a mirror plane in the molecule (Fig. 1a). In contrast, oxidative C–N coupling between asymmetric azaacenes, such as **BPO**, **BPT**, and 5,12-dihydro-5,12-diazatetracene (**DHDAT**),[14] gives chiral cruciform dimers with C–N axial chirality (Fig. 1b). Although there have been numerous examples of axially chiral C–C molecules represented by biaryl compounds,[15] including circularly polarized luminescence (CPL) emitters,[16–19] C–N axially chiral molecules have been less explored, probably because of the lower rotational barrier around the C–N bond compared to that around the C–C bond.[20] Among the axially chiral cruciform dimers of azaacenes, we hypothesize that the dimer of **BPO** (**1**) could be an interesting material because **BPO** is easily obtained on the gram scale by solid-state condensation of cheap compounds (2-aminophenol and 2,3-dihydroxynaphthalene). However, the optical resolution of **1** is difficult because of its low solubility, and the properties of its enantiomers remain unknown. In addition, the dimerization reaction of **BPO** requires a large amount of solvent owing to the low solubility of **BPO**. In this study, we designed a novel cruciform dimer **2**, which is a *tert*-butyl-substituted analogue of **1**, to achieve optical resolution and investigate the properties of the enantiomers by increasing their solubility. Furthermore, we aimed to synthesize **2** using mechanochemical oxidative coupling between **BPO** substituted with a *tert*-butyl group at the 2-position (**tBuBPO**) to achieve completely solvent-free synthesis of **2** from commercially available inexpensive chemicals.

Scheme 1 shows the synthesis of *rac*-**2**. **tBuBPO** was synthesized *via* a solid-state condensation reaction between 2-amino-

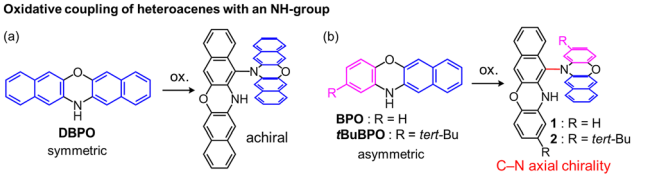

Fig. 1 (a) Achiral cruciform dimer formed by dimerization of symmetric azaacenes and (b) chiral cruciform dimers formed by dimerization of asymmetric azaacenes.

[a] *Department of Chemistry, Graduate School of Science, Osaka Metropolitan University, Sumiyoshi-ku, Osaka 558-8585, Japan. E-mail: sakamaki@omu.ac.jp, hfuji@omu.ac.jp*
[b] *Department of Polymer Chemistry, Graduate School of Engineering, Kyoto University, Nishikyo-ku, Kyoto 615-8510, Japan*

† Electronic supplementary information (ESI) available: Synthetic procedures, spectroscopic and computational data. CCDC 2332276–2332278. For ESI and crystallographic data in CIF or other electronic format see DOI: https://doi.org/10.1039/d4cc00977k

4-*tert*-butylphenol and 2,3-dihydroxynaphthalene at 230 °C, which is similar to the synthesis of **BPO**. Oxidation of **tBuBPO** with DDQ in dichloromethane afforded dimer *rac*-**2** in 73% yield. The dimerization of **tBuBPO** was also performed using a solvent-free mechanochemical oxidative coupling.[21–23] In a 50 mL stainless-steel jar of a mixer mill, **tBuBPO** (500 mg, 1.73 mmol) and DDQ (236 mg, 0.6 eq.) were placed with twelve stainless steel balls (10 mm ϕ) and milled at 30 Hz for 30 min. After purification by silica gel chromatography, 389 mg (78% yield) of compound *rac*-**2** was obtained. *Rac*-**2** is highly soluble in common organic solvents, in contrast to the very low solubility of **1**. For example, the solubility of *rac*-**2** in dichloromethane is ~45 mg mL^{-1}, which is nearly 100 times higher than that of **1** (*ca.* 0.5 mg mL^{-1}).

Recrystallization of *rac*-**2** by slow diffusion of methanol vapor into the toluene solution gave good single crystals suitable for X-ray crystal structure analysis. Fig. 2 shows the crystal structure of *rac*-**2**. In **2**, two **tBuBPO** units were almost planar, and the dihedral angle between them (*D*) was 83°. The unit cell contained one pair of enantiomers, and these molecules formed a centrosymmetric dimer by facing one **tBuBPO** moiety of **2** (Fig. 2c). In addition to π–π interactions, two intermolecular N–H/O hydrogen bonds (2.16 Å) were observed in the dimer. The enantiomer colored in light blue in Fig. 2c and d is the (*R*)-enantiomer, and the enantiomer colored in red is the (*S*)-enantiomer, according to the Cahn–Ingold–Prelog priority rules. However, the labeling of (*R*)- and (*S*)- of **BPO** dimers can be inverted, depending on the substituents on the **BPO** units (see ESI†). Therefore, for this class of cruciform dimers of azaacenes, we defined the enantiomer that gives (*M*,*M*)-double heterohelicenes upon intramolecular C–N bond formation as the (*M*)-enantiomer and the enantiomer that gives (*P*,*P*)-double heterohelicenes as the (*P*)-enantiomer, such that the configuration of the **BPO** skeletons and labeling always correspond, regardless of the substituents. According to this rule, the (*R*)-enantiomer (light blue in Fig. 2c and d) is defined as the (*M*)-enantiomer and the (*S*)-enantiomer (red in Fig. 2c and d) is defined as the (*P*)-enantiomer.

DFT calculations were performed for model compound of **2**, in which the *tert*-butyl groups were replaced by methyl groups. Structural optimization of model compound **2′** reproduced the molecular structure of **2** in the crystal well. Fig. S4 (ESI†) shows the frontier Kohn–Sham molecular orbitals (MOs) from HOMO−1 to LUMO+1, and their energies. The HOMO and LUMO are localized on different **BPO** units, similar to the cruciform dimer

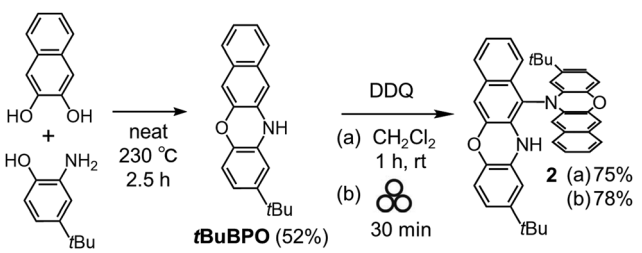

Scheme 1 Synthesis of **2**.

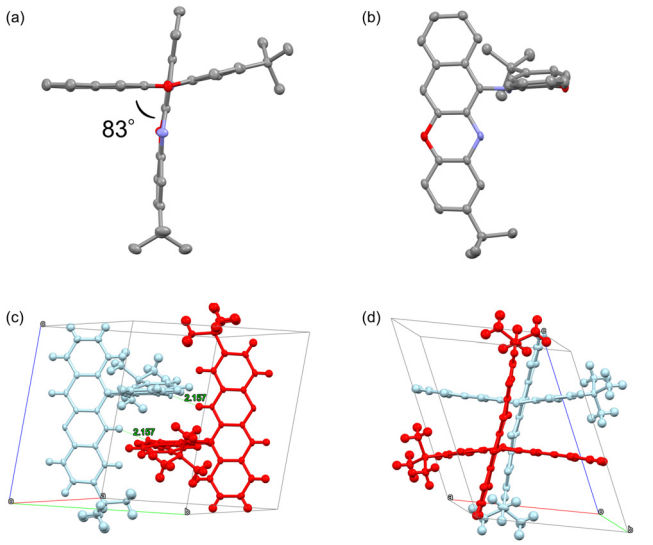

Fig. 2 (a) and (b) ORTEP representations of (*M*)-**2** in the racemic-crystal. (c) and (d) Packing structures of *rac*-**2**. Red and light blue in (c) and (d) represent the (*P*)- and (*M*)-isomers, respectively.

of 5,12-dihydro-5,12-diazatetracene.[14] The HOMO−1 and LUMO are distributed on the **BPO** unit with an NH group and the HOMO and LUMO+1 are distributed on the other **BPO** unit. The HOMO–LUMO transition was predicted to be nearly forbidden (f = 0.0001) because of the spatial separation of these MOs. The intramonomer transitions (HOMO−1 to LUMO and HOMO to LUMO+1) were predicted to have higher oscillator strengths.

The photophysical properties of *rac*-**2** and **tBuBPO** were then compared. The UV-vis absorption spectra of **2** and **tBuBPO** in dichloromethane were very similar (Fig. S5, ESI†). Both **2** and **tBuBPO** exhibited strong absorption peaks at approximately 370 nm, and their spectral shapes were similar. The band at 370 nm of **tBuBPO** was attributed to the HOMO–LUMO transition, and that of **2** was attributed to HOMO−1 to LUMO and HOMO to LUMO+1, according to the TD-DFT calculations. The peak corresponding to the HOMO–LUMO transition of **2** was not observed, as expected from TD-DFT calculations. Fig. 3a shows the emission spectra of **2** and **tBuBPO** in various solvents at room temperature. Both **2** and **tBuBPO** exhibited small bathochromic shifts with increasing solvent polarity, and the emission peaks of **2** were slightly red-shifted compared with those of **tBuBPO** in each solvent. The red-shifted emission of **2** can be explained by the contribution of the HOMO–LUMO transition with an intermonomer transition character to the $S_1 \rightarrow S_0$ transition. The solutions of *rac*-**2** and **tBuBPO** in all solvents tested exhibited blue emission owing to small solvatochromism, and the emission quantum yields of **2** ranged from 40% (in THF) to 17% (in dichloromethane), comparable to those of **tBuBPO** (Fig. 3b).

We measured the temperature dependence of the emission spectra of *rac*-**2** and **tBuBPO** in 2-MeTHF upon cooling from room temperature (Fig. S6, ESI†). **2** exhibited broad emission band at approximately 410 nm at 293 K. Upon cooling from 293 K, vibronic patterns appeared gradually without significant

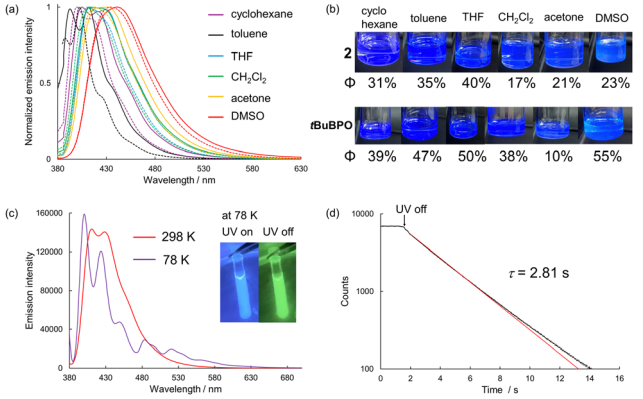

Fig. 3 (a) Solvent dependence of emission spectra of *rac*-**2** (solid lines) and **tBuBPO** (dotted lines) at room temperature. (b) Photographs of the solutions of *rac*-**2** and **tBuBPO** in various solvents taken under irradiation with UV light at 365 nm and their emission quantum yields. (c) Emission spectra of **2** in 2-MeTHF measured at 298 K and 78 K. (inset) Photographs of the solutions of *rac*-**2** taken under irradiation with UV light at 365 nm and just after turning it off at 78 K. (d) Emission decay curve (at 520 nm) of *rac*-**2** in 2-MeTHF measured at 78 K. Red line is the fitting curve using first order decay curve.

changes in the emission wavelength. Upon cooling below 93 K, new emission bands appeared in the longer-wavelength region at approximately 500 nm (Fig. 3c). The newly appearing emission was attributed to phosphorescence, based on the long afterglow that could be observed in green with the naked eye for approximately 10 s, and the lifetime at 520 nm was 2.8 s (Fig. 3d). The temperature dependence of the emission of **2** was similar to that of **tBuBPO**; however, the phosphorescence lifetime of **2** was longer than that of **tBuBPO** (2.2 s).

Optical resolution of the cruciform **BPO** dimer without *tert*-butyl groups (**1**) was not achieved owing to its low solubility in the mobile phase of chiral column chromatography. In contrast, the enantiomers of **2** were successfully separated using a chiral column equipped with high-performance liquid chromatography (HPLC) owing to their increased solubility (Fig. S7, ESI†). Single crystals of each enantiomer suitable for X-ray analysis were successfully obtained. X-ray single crystal analysis revealed that the faster eluting enantiomer was the (*M*)-isomer, and the slowly eluting enantiomer was the (*P*)-isomer. In the crystals, each enantiomer formed a dimer by facing the **tBuBPO** units, similar to *rac*-**2**; however, in this case, the two *tert*-butyl groups of the stacked **tBuBPO** units were on the same side (Fig. S9, ESI†). Two intermonomer N–H/O hydrogen bonds (2.30 and 2.02 Å) were observed in the dimer.

We measured the circular dichroism (CD) spectra of the enantiomers of **2** in dichloromethane. As shown in Fig. 4a, the enantiomers exhibited mirror-image CD spectra. The (*P*)-enantiomer exhibited the first positive Cotton effect, and the observed spectra were well reproduced by TD-DFT calculations at the PBE0/6-31G(d) level of theory, except for systematic overestimation of the transition energies. Interestingly, the sign of the first Cotton band of (*P*)-**2** was opposite to that of the (*P*,*P*)-enantiomer of double hetero[5]helicene (**BPO-DH**) composed of two **BPO** obtained by ring fusion of (*P*)-**1**;[10] that

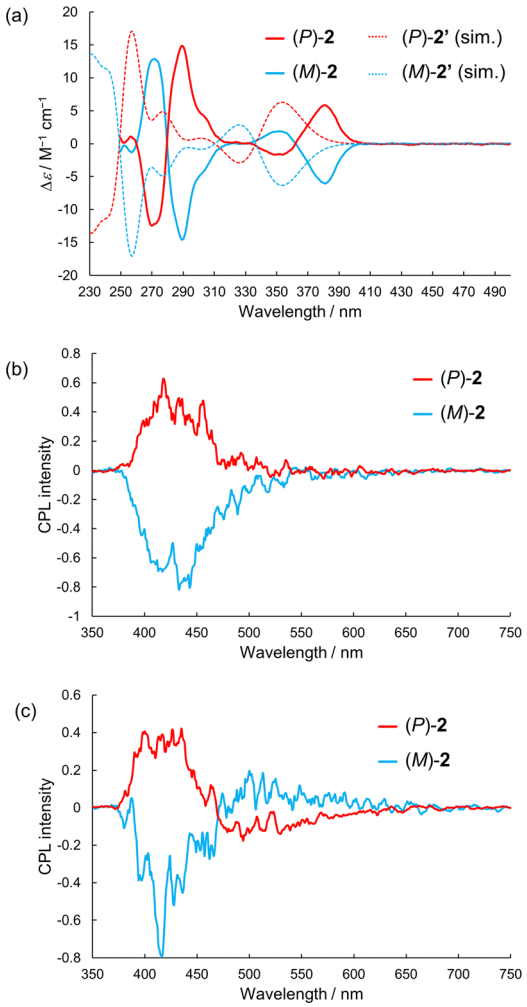

Fig. 4 (a) CD spectra of **2** in dichloromethane at room temperature and TD-DFT simulated spectra of **2**′ calculated at the PBE0/6-31G(d) level of theory. (b) and (c) CPL spectra of **2** in dichloromethane at 298 K and in 2-MeTHF at 83 K, respectively.

is, the conversion from a cruciform dimer to a double hetero[5]helicene by intramolecular C–N bond formation inverted the signs of the first Cotton band. The $|g_{CD}|$ value of **2** was 1.4×10^{-3} at 385 nm, which is comparable to those of previously reported axially chiral CPL emitters.[16,18,19]

To evaluate the racemization barrier of **2**, we monitored temporal changes in the CD intensity of the enantiomer of **2** in toluene at 92.5, 95, 97.5, and 100 °C. The CD intensity slowly decreased with first-order kinetics (Fig. S10, ESI†) and the rate constants were determined for each temperature. The racemization barrier of **2** was estimated to be 149 ± 20 (standard error) kJ mol^{-1} from the Arrhenius plot using the obtained rate constants. This value is sufficiently high to ignore racemization at room temperature.

Next, we measured the CPL spectra of the enantiomers of **2**. Fig. 4b shows the CPL spectra in dichloromethane at 298 K. Mirror-image CPL spectra were obtained at approximately 420 nm, which can be attributed to fluorescence. The (*P*)-enantiomer exhibited a positive CPL, which was in accordance

with the first Cotton effect of the (*P*)-enantiomer in the CD spectrum. The experimental $|g_{CPL}|$ value was approximately 6×10^{-4}. TD-DFT calculation for the optimized S_1 structures reproduced the signs of g_{CPL} (Table S4, ESI†). Interestingly, TD-DFT calculations suggested that the g_{CPL} values could be significantly affected by the dihedral angle between the two **tBuBPO** units (Table S5, ESI†). The calculated g_{CPL} value of (*P*)-**2** at the optimized S_1 geometry (dihedral angle: $D = 99.7^\circ$) was $+2.0 \times 10^{-2}$; however, the magnitude of g_{CPL} decreased with increasing *D*. Upon decreasing *D*, the sign of g_{CPL} was inverted between $D = 95^\circ$ and 92.5°. Next, we measured the CPL spectra of the enantiomers of **2** in frozen solutions of 2-MeTHF at 83 K, because **2** exhibited phosphorescence upon cooling. New CPL peaks at approximately 500 nm, with signs opposite to those of CPL fluorescence at 420 nm at 83 K (Fig. 4c). Based on the emission lifetime of 2.8 s at 520 nm, the newly appeared CPL at 83 K was attributed to phosphorescence. The $|g_{CPL}|$ value of phosphorescence was *ca.* 1×10^{-3} at 550 nm (Fig. S11, ESI†).

In summary, we synthesized a novel C–N axially chiral compound composed of two *tert*-butyl-substituted benzo[*b*]-phenoxazines, which can be obtained using only solvent-free reactions from commercially available compounds. The introduction of *tert*-butyl groups significantly increased the solubility of the cruciform dimer in common organic solvents, and we succeeded in the optical resolution of this class of dimers for the first time. We demonstrated that the enantiomers of **2** have a sufficiently high racemization barrier even when the NH group is not substituted with a bulky substituent. **2** exhibited moderate emission quantum yields in various solvents and long-lived phosphorescence upon cooling. The enantiomers of **2** showed clear CPL at room temperature and dual CPL originating from fluorescence and phosphorescence at liquid-nitrogen temperature. We believe that this study will lead to novel design concepts for chiral emitters and catalysts for enantioselective syntheses that can be easily obtained *via* solvent-free reactions.

This work was supported by a Grant-in-Aid for Scientific Research (17H04874, 18K05264, 20H02726) from the Japan Society for the Promotion of Science (JSPS), a Grant-in-Aid for Transformative Research Areas (A) ''Condensed Conjugation'' (JSPS KAKENHI Grant Number JP20H05866) from MEXT, Ogasawara Toshiaki Memorial Foundation, Shorai Foundation for Science and Technology, The Foundation for the Promotion of Ion Engineering, and Izumi Science and Technology Foundation. Computation time for the theoretical calculations was provided by Research Center for Computational Science, Okazaki, Japan.

Conflicts of interest

There are no conflicts of interest to declare.

Notes and references

1 T. Hatakeyama, K. Shiren, K. Nakajima, S. Nomura, S. Nakatsuka, K. Kinoshita, J. Ni, Y. Ono and T. Ikuta, *Adv. Mater.*, 2016, **28**, 2777–2781.
2 M. Mamada, M. Hayakawa, J. Ochi and T. Hatakeyama, *Chem. Soc. Rev.*, 2024, **53**, 1624–1692.
3 M. Watanabe, H. Hagiwara, A. Iribe, Y. Ogata, K. Shiomi, A. Staykov, S. Ida, K. Tanaka and T. Ishihara, *J. Mater. Chem. A*, 2014, **2**, 12952–12961.
4 A. F. Buene and D. M. Almenningen, *J. Mater. Chem.*, 2021, **9**, 11974–11994.
5 S. Dadashi-Silab, X. Pan and K. Matyjaszewski, *Chem. – Eur. J.*, 2017, **23**, 5972–5977.
6 F. Seyfert and H.-A. Wagenknecht, *Synlett*, 2021, 582–586.
7 S. Shibutani, T. Kodo, M. Takeda, K. Nagao, N. Tokunaga, Y. Sasaki and H. Ohmiya, *J. Am. Chem. Soc.*, 2020, **142**, 1211–1216.
8 S. Halder, S. Mandal, A. Kundu, B. Mandal and D. Adhikari, *J. Am. Chem. Soc.*, 2023, **145**, 22403–22412.
9 D. Sakamaki, D. Kumano, E. Yashima and S. Seki, *Angew. Chem., Int. Ed.*, 2015, **54**, 5404–5407.
10 D. Sakamaki, S. Tanaka, K. Tanaka, M. Takino, M. Gon, K. Tanaka, T. Hirose, D. Hirobe, H. Yamamoto and H. Fujiwara, *J. Phys. Chem. Lett.*, 2021, 9283–9292.
11 D. Sakamaki, D. Kumano, E. Yashima and S. Seki, *Chem. Commun.*, 2015, **51**, 17237–17240.
12 S. Tanaka, D. Sakamaki, N. Haruta, T. Sato, M. Gon, K. Tanaka and H. Fujiwara, *J. Mater. Chem.*, 2023, **11**, 4846–4854.
13 D. Sakamaki, Y. Inoue, K. Shimomura, D. Taura, E. Yashima and S. Seki, *Tetrahedron Lett.*, 2023, **114**, 154294.
14 K. Tanaka, D. Sakamaki and H. Fujiwara, *Chem. – Eur. J.*, 2021, **27**, 4430–4438.
15 G. Bringmann, A. J. Price Mortimer, P. A. Keller, M. J. Gresser, J. Garner and M. Breuning, *Angew. Chem., Int. Ed.*, 2005, **44**, 5384–5427.
16 K. Hassan, K.-I. Yamashita, K. Hirabayashi, T. Shimizu, K. Nakabayashi, Y. Imai, T. Matsumoto, A. Yamano and K.-I. Sugiura, *Chem. Lett.*, 2015, **44**, 1607–1609.
17 K. Takaishi, R. Takehana and T. Ema, *Chem. Commun.*, 2018, **54**, 1449–1452.
18 K. Takaishi, S. Hinoide, T. Matsumoto and T. Ema, *J. Am. Chem. Soc.*, 2019, **141**, 11852–11857.
19 K. Takaishi, T. Matsumoto, M. Kawataka and T. Ema, *Angew. Chem., Int. Ed.*, 2021, **60**, 9968–9972.
20 Z.-S. Liu, P.-P. Xie, Y. Hua, C. Wu, Y. Ma, J. Chen, H.-G. Cheng, X. Hong and Q. Zhou, *Chem. – Eur. J.*, 2021, **7**, 1917–1932.
21 S. Grätz, D. Beyer, V. Tkachova, S. Hellmann, R. Berger, X. Feng and L. Borchardt, *Chem. Commun.*, 2018, **54**, 5307–5310.
22 S. Grätz, M. Oltermann, E. Troschke, S. Paasch, S. Krause, E. Brunner and L. Borchardt, *J. Mater. Chem. A*, 2018, **6**, 21901–21905.
23 H. Sada, D. Sakamaki, M. Gon, K. Tanaka, T. Hirose and H. Fujiwara, *ChemRxiv*, 2024, DOI: 10.26434/chemrxiv-2024-sbv85.